Hindawi
Shock and Vibration
Volume 2021, Article ID 9911135, 11 pages
https://doi.org/10.1155/2021/9911135

Research Article

Frequency-Based Control Strategy for Compact Electromagnetic Tuned Mass Damper

Semen Kopylov,[1] **Zhaobo Chen**,[1] **and Mohamed A. A. Abdelkareem**[2]

[1]*Harbin Institute of Technology, Harbin 150001, China*
[2]*Automotive and Tractors Engineering Department, Faculty of Engineering, Minia University, El-Minia 61519, Egypt*

Correspondence should be addressed to Semen Kopylov; kopiloffsemen@yandex.ru

Received 22 March 2021; Revised 10 April 2021; Accepted 26 April 2021; Published 4 May 2021

Academic Editor: Marcos Silveira

The control of harmonic machine-induced vibration has been a common task in the engineering scope. The passive tuned mass dampers represent the most reliable and practical approach to reduce such excessive vibration. Additionally, different control strategies can be implemented on TMDs to improve the attenuation performance further. However, most of the proposed control strategies for TMDs represent cost and complex systems with many sensors, which hinders the broad implementation. In this paper, the frequency-based semiactive control (FBC) strategy was proposed for an electromagnetic tuned mass damper (ETMD). The concept of a controllable system with switched transistor was utilized for the proposed control strategy. The proposed control policy's effectiveness was validated by experimental results, where the controlled ETMD was applied on a protected mass test bench. This paper concluded that the proposed control strategy has a significant advantage over the passive TMD. The reduction of 14% of the excessive harmonic vibration for the protected structure was observed.

1. Introduction

Undesirable machine-induced vibrations with a harmonic nature can cause serious damage to mechanisms and structures. That kind of vibration can be induced by rotating machinery such as engines, driveshafts, flywheels, and rotors. As passive vibration absorption devices are limited to a specific narrow operation frequency bandwidth to reduce the unwanted influence of machine-induced vibrations, different control techniques under harmonic-based vibrations have been proposed, implemented, and investigated over decades. Takamoto et al. [1] proposed a new method by integrating model predictive and semiactive controls, and such a control strategy is known as predictive switching based on harmonic input (PSHI). The PSHI predicted the system's future states by assuming the harmonic control inputs and harmonic disturbances that caused resonance. Wang [2] developed an active restricted control for harmonic vibration suppression. The study case demonstrated the feasibility of the proposed approach. Such control allows the reduction of vibration for systems where the numbers of sensors and actuators are limited. Harmonic vibrations induced by the unbalanced rotor of a magnetically suspended flywheel represent a challenge for control engineers. To suppress the harmonic vibrations for such systems, a compound control method was proposed by Zhang et al. [3]. The generalized notch filter and the repetitive control method are mainly adopted to suppress the harmonic vibration caused by sensor runout and rotor unbalance. That approach indicated the reduction of first- and fifth-order harmonic vibration of the given system by at least 70% and 50%, respectively. Tuned mass dampers (TMDs) are, on the other hand, one of the most robust, basic, and yet efficient passive approaches to suppress harmonic vibrations [4]. For such a case, the additional mass is mounted on the structure needed to protect unwanted vibration. TMDs can be adopted for both rectilinear vibration applications and angular rotational applications. Thus, TMDs have a broad range of applications. For instance, Nerubenko et al. [5] proposed an energy harvesting tuned mass damper in the

vehicle driveline. The developed device could reduce the harmonic vibration levels for the driveline shaft and effectively harvest the wasted vibration energy to feed autonomous wireless devices.

The traditional passive TMD with a fixed frequency cannot work effectively in the width range of frequency variations. Therefore, specific control techniques for TMDs were proposed to improve the application's performance in various cases. Gao et al. [6] proposed a frequency-adjustable tuned mass damper (FATMD) to solve this limitation of the traditional passive TMD for structural vibrations. The numerical results indicated that the proposed FATMD could reduce the pedestrian bridge's vertical vibration under the excitations of pedestrians, escalators, and earthquakes. Beltran-Carbajal [7] proposed a novel active vibration strategy to extend a passive TMD's vibration suppression capability. The proposed system includes a feedback controller for reference position trajectory tracking tasks on the vibration absorber and an online asymptotic estimation approach of harmonic excitation forces and its time derivatives of a certain order. Based on the simulation results, the fast and effective estimation of the harmonic perturbation forces is verified.

A new control algorithm for semiactive tuned mass dampers (STMDs) with magnetorheological (MR) dampers was experimentally evaluated by Maslanka [8]. In another study, Nishimura et al. [9] proposed an acceleration feedback control, and the controller performance was optimized and modified. The simulations demonstrated that the presented semiactive control algorithm enables the STMD to achieve similar performance to that of the TMD with five times larger mass.

It is noteworthy that the absorption of random vibrations in civil engineering is a classic application for TMDs. In this sense, various control mechanisms for reducing seismic and wind loads from civil structures have been proposed. STMD was proposed by Chey et al. [10] to mitigate structural response due to seismic loads. The STMD system with a reasonable combination of TMD parameters was found to provide better control than the passive system. Due to additional TMD damping provided at optimal damping values that may be unattainable, the acceleration response reduction of the passive system is slightly greater than that of the STMD system. Aldemir [11] used an MR damper to implement the best control for the TMD when it was subjected to a variety of seismic inputs. For all cases studied, the proposed approach is always better than the equivalent passive TMD. Except for the aforementioned semiactive control strategy for TMDs, various approaches have been investigated and implemented for TMD, such as clipped linear quadratic regulator (LQR) [12, 13], linear quadratic Gaussian control (LQG) [14, 15], variations of ground hook control schemes [16, 17], and on-off phase control algorithms [18, 19].

The control algorithm requires a considerable amount of time and memory for online computation since the deemed semiactive techniques involve the solution of differential equations. Thus, such strategies are less dependable and costly [20]. Furthermore, full state feedback is required, which demands the use of more sensors, increasing device complexity and expense. Therefore, the frequency-based control strategy was suggested in this paper as a simplified and more efficient semiactive control strategy for TMDs. The novel idea is inspired by a TMD system's invariant points property and needs only one accelerometer. The technique aims to reduce repetitive harmonic vibrations on a safe frame.

The paper is organized as follows: the mathematical model and control strategy are explained in Section 2. The experimental configuration is then presented. The experimental findings of the proposed control strategy on an electromagnetic tuned mass damper are presented in Section 3. Finally, the key contributions of the paper were outlined and concluded in Section 4.

2. Materials and Methods

2.1. Mathematical Modeling. To begin, consider the traditional TMD configuration, in which the TMD is placed on a secured structure using a conventional damper and coil spring, as shown in Figure 1.

According to Newton's second law, the equations of motion of the given 2-DOF with the TMD model are as follows:

$$\left\{ \mathbf{M}\ddot{\mathbf{y}}_1 - \mathbf{c}\dot{\mathbf{z}}_2 + \mathbf{K}\mathbf{y}_1 - \mathbf{k}\mathbf{z}_2 = \mathbf{K}\boldsymbol{\eta}(\mathbf{t})\mathbf{m}\ddot{\mathbf{z}}_2 + \mathbf{m}\ddot{\mathbf{y}}_1 + \mathbf{c}\dot{\mathbf{z}}_2 + \mathbf{k}\mathbf{z}_2 = 0, \right. \tag{1}$$

where M is the protected structure incorporated with a spring stiffness K. The TMD device is depicted as a piece of mass m with a spring stiffness k and a viscous damping c. The system is exposed by a kinetic excitation of $\eta(t)$. The relative displacement between the TMD and the protected structure is represented by $z_2 = y_2 - y_1$.

In this case, the optimized damping and stiffness coefficients for the best attenuation efficiency can be extracted using the optimization techniques described in [21]. As seen in Figure 2, Kopylov et al. [22] suggested an electromagnetic TMD model in which the damping coefficient can be varied by adjusting the load resistance in the electrical circuit.

The viscous damping force f_{EMF} produces an electromotive force e_{EMF} in the electrical circuit, representing the equivalent of the damping force. R_{load} and R_{coil} are the external load resistance and the TMD inherent coil resistance, respectively, while L_{coil} donates the TMD inherent coil inductance. Referring to Figure 2, according to Kirchhoff's law for electrical circuits, equation (2) is obtained:

$$\mathbf{L}_{\mathbf{coil}} = \frac{\mathbf{di}}{\mathbf{dt}} + \mathbf{Ri} - \mathbf{k}_{\mathbf{t}}\dot{z}_2 = 0, \tag{2}$$

where k_t is an electromechanical coupling coefficient which also could be written as $k_t = NBl$. N is the number of coil turns, while B is the average magnetic flux density in the air gap and l is the coil length across the magnetic flux. R consists of the coil resistance and an external load, respectively, as $R = R_{\mathrm{coil}} + R_{\mathrm{load}}$.

Then, according to Lenz's law and Ohm's law, the electrical damping coefficient of the TMD is

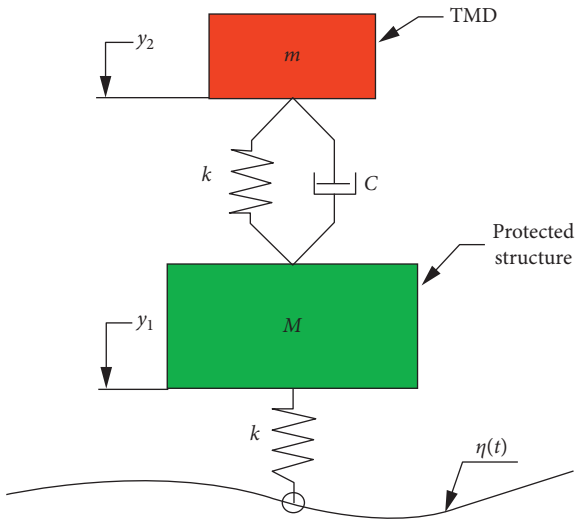

Figure 1: Mathematical model of the typical TMD implementation.

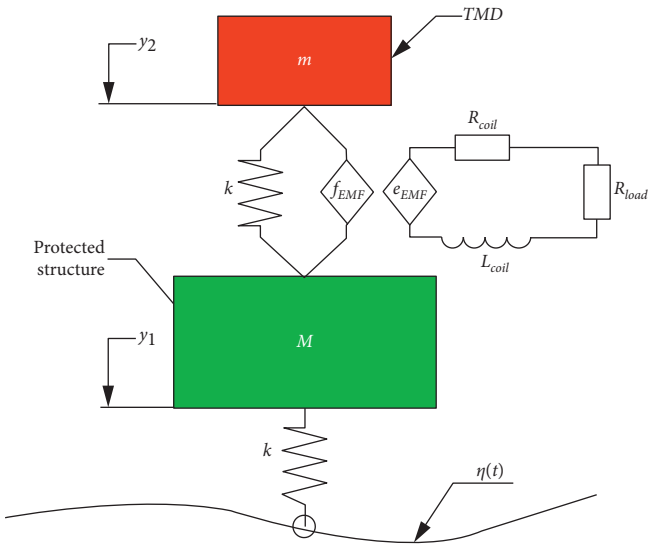

Figure 2: Mathematical model of the electromagnetic TMD implementation.

$$\mathbf{d_e} = \frac{\mathbf{k_t^2}}{\mathbf{R_{coil} + R_{load}}} = \frac{(\mathbf{NBl})^2}{\mathbf{R_{coil} + R_{load}}}. \tag{3}$$

The total damping coefficient c consists of d_e and d_m, where d_e is the electrical damping coefficient (as given in equation (3)), and the mechanical or heat loss damping is symbolled by d_m. It is worth remembering that the damping in equation (3) holds true even though the inductance effects are negligible. The suggested design can be thought of as an electromechanical system with R circuit (EMR) [23]. A circuit like this adds damping between the TMD and the secured structure physically.

Equation (3) shows that the electrical damping is inversely proportional to the external load resistance while mechanical damping, coil resistance, and coupling coefficient are all constants. Thus, an electrical circuit with an adjustable resistor is needed to achieve semiactively regulation of the damping force for such a device. As seen in Figure 3, Ning et al. [24] suggested an approach based on the metal-oxide semiconductor field-effect transistor (MOSFET).

When the MOSFET is turned on, it supplies the circuit with the lowest load resistance (about 0.3 ohms), resulting in the system's highest electrical damping coefficient (as given in equation (3)). Otherwise, the system's electrical damping coefficient is likely to be negative. The ON state is represented by a high-level voltage on the MOSFET's gate, while the OFF condition is represented by a low-level voltage. The controller is used to generate a voltage based on the control technique. Since current may only pass from drain to source via the N-channel MOSFET, the rectifier is used to provide current in the correct direction.

In this article, the suggested technique is used to achieve semiactive control dependent on excitation frequency. The amplitudes of the covered structure and the TMD were used as success criteria to test the efficiency of the proposed control strategy under harmonic excitation. The transition functions between the excitation and the output criteria can be obtained by solving the differential equations in equation (1). The following is the transfer function between excitation and amplitude of the covered structure:

$$\mathbf{H_{ps}(s)} = \frac{\mathbf{K}\left(\mathbf{cs} + \mathbf{ms}^2 + \mathbf{k}\right)}{\mathbf{D(s)}},$$
$$\mathbf{D(s)} = \mathbf{Mms}^4 + \mathbf{cs}^3(\mathbf{M} + \mathbf{m}) + \mathbf{s}^2(\mathbf{Km} + \mathbf{Mk} + \mathbf{km}) + \mathbf{Kcs} + \mathbf{Kk}. \tag{4}$$

The transfer function between the excitation and the TMD relative amplitude z_2 is as follows:

$$\mathbf{H_{TM\,D}(s)} = \frac{-\mathbf{K} \cdot \mathbf{m} \cdot \mathbf{s}^2}{\mathbf{D(s)}}. \tag{5}$$

2.2. Control Strategy Explanation

2.2.1. Control Strategy Concept Based on the TMD Theory. This paper proposes a novel semiactive control technique for protected structures subjected solely to harmonic excitations. The concept is based on the TMD system's invariant points property (see Figure 1). The ordinates of its appearance on the frequency response are invariant points that are unaffected by damping. As seen in Figure 4, the frequency curve of the covered system intersects at these points, corresponding to various viscous coefficients of the TMD.

It is worth noting that Den Hartog [25] suggested the classical approach of optimizing the damped TMD based on this property. The optimal solution of a system with a TMD without damping (blue dashed line) is in the frequencies between the invariant points and as seen in Figure 4. The undamped TMD has not been widely used because of the undesirable response in the frequency spectrum outside of the invariant points. Therefore, optimized damping systems

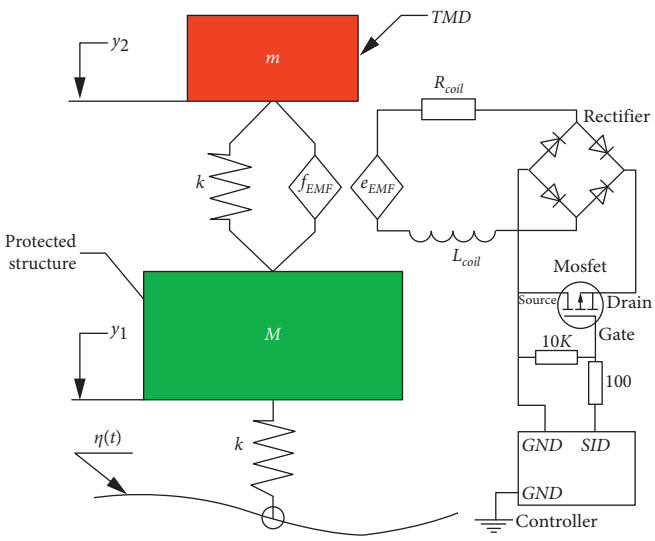

Figure 3: Schematic diagram of the controllable damping TMD system.

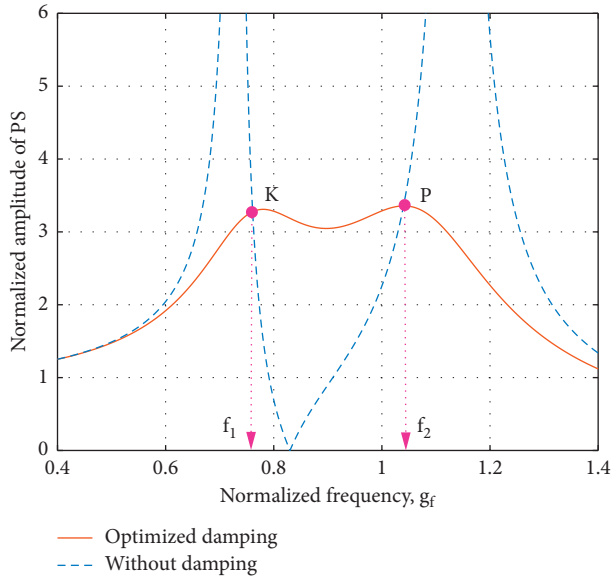

Figure 4: Amplitude-frequency response of the protected structure.

have been introduced as systems with a rational response in a specific frequency bandwidth (solid red line). However, the optimized damping systems do not perform much better than the undamped TMD case between invariant points. The semiactive frequency-based control (FBC) technique was formulated in this regard.

The FBC technique attempts to control the damping force of the TMD system depending on the excitation frequency so that the TMD system must be totally undamped during the time of excitation with frequencies located between invariant points. The optimized damping is used for frequencies that are outside of the spectrum of the invariant points. The amplitude-frequency response of the TMD system's safe configuration is calculated using equation (4). The optimized damping reaction of the covered structure is depicted by the solid red line in Figure 4, while the undamped case of the TMD is represented by the blue dashed line. As seen in Figure 4, the protected structure response between the invariant points K and P with the corresponding frequencies f_1 and f_2 is the best for the undamped TMD case, while out of this range, the optimized damping TMD performs better. Then, to obtain the values of the frequencies f_1 and f_2, the horizontal coordinates of the invariant points are derived from equation (4) by equating the undamped response with the optimized damping response of the protected structure. Thus, the positive roots of this equation equivalent to the corresponding frequencies of the invariant points in terms of mass ratio and properties of the TMD and protected structure can be obtained as in equation (6). The parameters of the system are listed in Table 1.

$$\mathbf{g}_{\mathbf{f}_{1,2}} = \pm\left(\frac{2\boldsymbol{\pi}\sqrt{(\boldsymbol{\mu}+2)\left(\mathbf{f}^2\boldsymbol{\mu}+\mathbf{f}^2+\sqrt{\left(1+(\boldsymbol{\mu}+1)^2\mathbf{f}^4-2\mathbf{f}^2\right)}+1\right)}}{(\boldsymbol{\mu}+2)}\right). \tag{6}$$

The coordinates for these invariant points are obtained for the case with negligible inductance effects. However, in a case of significant inductance effects, the TMD system will be represented as a Zener model with spring and dashpot linked in series [26, 27]. That model requires a different algorithm for finding the coordinates of the invariant points.

2.2.2. Control Algorithm. According to the FBC technique, processing the signal from the accelerometer connected to the protected structure helps to calculate the excitation frequency of the system. The damping force of the TMD can then be set to be minimal depending on the derived value of the frequency if the frequency is in the range located between the invariant points. Otherwise, as defined in Section 2.1, the damping force is set to maximum by switching the MOSFET transistor. Therefore, the law of the FBC strategy has become

$$u_{fbc} = \begin{cases} c_a = c_{a,\max}, & \text{for } f_m \le f_1 \text{ or } f_m \ge f_2 \\ c_a = 0, & \text{for } f_1 < f_m < f_2 \end{cases}, \tag{7}$$

where f_m is a measured excitation frequency from the acceleration signal and c_a donates the adjustable damping of the TMD. The program code of the control algorithm and the process of deriving the excitation frequency of the system from the protected structure vertical acceleration data are represented in Algorithm 1.

2.3. Experimental Setup. The architecture of the electromagnetic TMD suggested by the author in previous work is used in this paper for experimental validation. Figure 5 depicts the construction principles of the back-iron design-based electromagnetic TMD. The TMD was mounted on the protected structure via a connecting flange. As Figure 6(a) shows, the protected structure is a cylindrical piece of steel incorporated with the coil spring.

Table 1: Parameters of the TMD system.

Equation	Description
$\mu = (m/M)$	The mass ratio (absorber mass/main mass)
$\omega_{TMD} = \sqrt{(k/m)}$	The natural frequency of a TMD
$\Omega_{PS} = \sqrt{(K/M)}$	The natural frequency of a protected structure
$f = (\omega_{TMD}/\Omega_{PS})$	The frequency ratio (natural frequencies)
$g_f = (\omega/\Omega_{PS})$	The forced frequency ratio

```
 //Connecting libraries:
#include <avr/io.h>
#include <avr/interrupt.h>
//Pin definition:
//Acceleration Input:
const int Acc_1 = A2;
const int Acc_2 = A1;
//Control output:
const int SWITCH1 = 4;
//Variables:
float f = 0; //frequency of the system excitation;
int VA_1; //the first measured acceleration;
int VA_2; //the second measured acceleration;
unsigned int timerValue; //timer value; //Start the code:
void setup() {

 cli(); //cancell general interupptions
 pinMode(SWITCH1, OUTPUT);
 // setting the timer 1:

TCCR1A = 0;
TCCR1B = 0;
TCCR1B |= (1 << CS10);
TCCR1B |= (0 << CS11);
TCCR1B |= (1 << CS12); //start up the timer }
void loop() {

 VA_1 = analogRead(Acc_1); //reading accelerator sensor data;
 VA_2 = analogRead(Acc_2); //reading accelerator sensor data;
 if (VA_1 > 440 && VA_2 ≤ 440){
 TCCR1B |= (0 << CS10);
 TCCR1B |= (0 << CS11);
 TCCR1B |= (0 << CS12); //stop the timer

  timerValue = (unsigned int)TCNT1L | ((unsigned int)TCNT1H << 8); //reading the timer;

 f = 1/((float)(timerValue) * 0.000064); //deriving the frequency;
 TCNT1H = 0; //resetting the timer;
 TCNT1L = 0; TCCR1B |= (1 << CS10);
 TCCR1B |= (1 << CS12);
 //set the resolution of the timer with a divider 1024; //FBC control law:
 if (f ≥ 8.2 && f ≤ 10){

  digitalWrite(SWITCH1,LOW); //set the maximum damping of the TMD;

 }
 else {

  digitalWrite(SWITCH1,HIGH); //set the minimum damping of the TMD;

 }
 }

  VA_1 = 0;
  VA_2 = 0; }
```

Algorithm 1

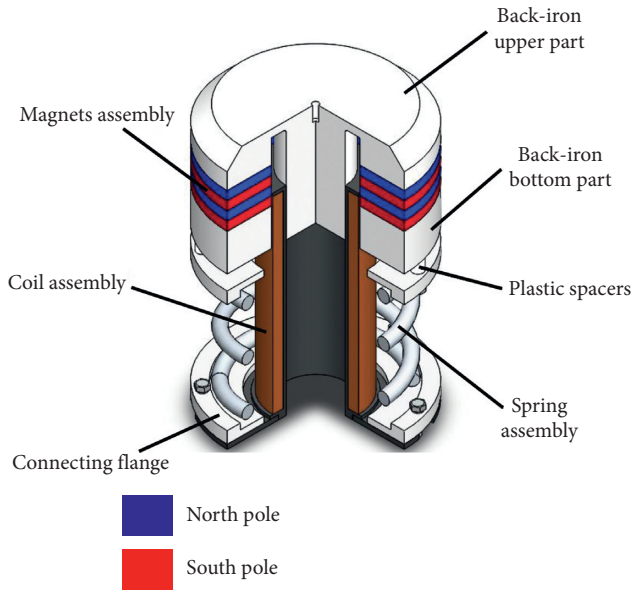

Figure 5: Back-iron design-based electromagnetic TMD [22].

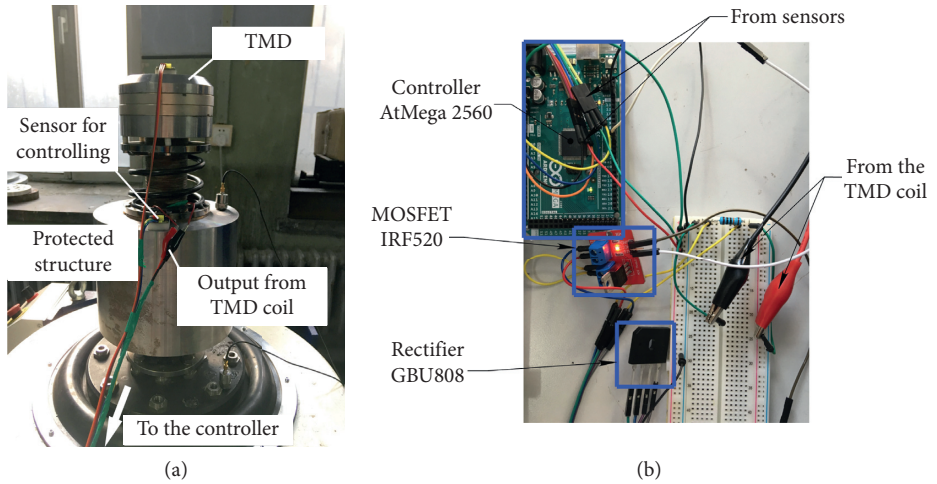

Figure 6: (a) Setup of the 2-DOFs TMD prototype fixed in the protected structure. (b) Experimental layout of the control circuit.

To derive the system's amplitude-frequency response, two piezoelectric accelerometers (AD100S) were fixed on both the TMD moving part and the protected structure, as shown in Figure 6(a). The schematic layout of the experimental setup including both the TMD and the control circuit is given in Figure 6(b). The AtMega 2560 controller was exploited to process the measurements from accelerometers and then to accomplish the control algorithm. The MOSFET IRF520 was parallelly connected to the TMD coil through a rectifier (GBU808). The general schematic layout of the experimental setup is shown in Figure 7. All the parameters of the 2-DOF TMD fabricated prototype system are listed in Table 2.

The exploited excitation equipment consists of a vibration controller VT-9008 and a data acquisition platform. The ETS Solutions company's vibration excitation machine no. MPA403/M124A was used to generate harmonic excitation with a frequency sweep from 5 to 15 Hz. The results of the established experiment are represented in the next section.

3. Experimental Results

The 2-DOF TMD model is built to demonstrate the performance of the proposed FBC strategy compared with that of the passive TMD system. To estimate the performance of each case reasonably, two indices were introduced. The first one is the peak index I_P which indicates the maximum value of the response for the considered range of frequencies. Secondly, the average value I_a of the response for the considered range of frequencies is represented as follows:

$$\mathbf{I_a} = \frac{1}{(\mathbf{f_u} - \mathbf{f_l})} \int_{\mathbf{f_l}}^{\mathbf{f_u}} \mathbf{H}(\mathbf{s})\mathbf{ds}, \tag{8}$$

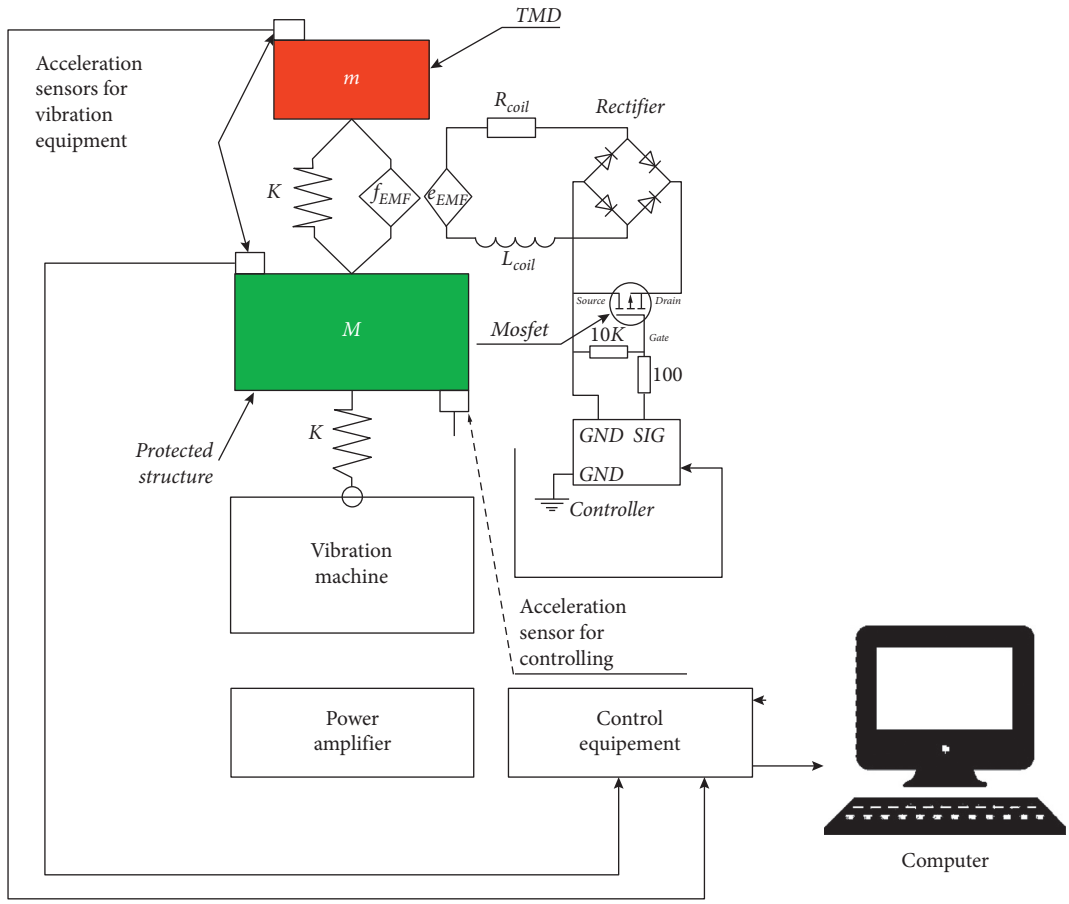

Figure 7: Experimental schematic layout of the TMD.

Table 2: Parameters of the 2-DOF TMD model.

Parameter	Symbols	Value
Mass of the protected structure	M	41.5 kg
Mass of the TMD	M	5.5 kg
Stiffness of the protected structure	K	172827 N/m
Stiffness of the TMD	K	18426 N/m
Resistance of the coil	R_{coil}	513.5 Ω
Inductance of the coil	L_{coil}	1.27 H
Number of windings	N	9400
Length of the coil	L	1475.8 m
Electromechanical coupling coefficient	k_t	182.3 T·m

where f_l and f_u donate the lower and upper limits of the considered frequencies, respectively.

To validate the proposed passive TMD system in the protected structure test-bench implementation, the passive TMD performance was evaluated for three study cases under harmonic excitation with a frequency range from 5 to 10 Hz, and an amplitude of $250 * 10^{-6}$ m: (1) open circuit case without damping; (2) damping $de = 32.8$ N·s/m corresponding to the external resistive load $R_{\text{load}} = 500$ Ohm; and (3) short circuit case when the damping coefficient is maximum at de = 64.7 N·s/m. As it may cause damage to the protected structure, the case without TMD was not considered. By differentiating the signal derived from the accelerometers, which are depicted in Figure 7, the protected structure and TMD's amplitude response were obtained, as shown in Figure 8.

It was confirmed that with increasing the damping coefficient of the passive TMD, the amplitude of the protected structure was reduced considerably. As seen in Figure 8, the peak index I_P decreased by 71% when considering the two cases with full usable damping (solid green line) and without damping (dashed red line). The device with passive and operated TMD was then subjected to harmonic excitation with a frequency range of 6–14 Hz and an amplitude of $125 * 10^{-6}$ m to demonstrate the benefit of using the proposed FBC strategy. Figure 9 shows the related amplitude-frequency responses of the covered structure mass for both the passive and FBC controlled scenarios.

It is seen that such a control policy indicated considerable improvements in the protected structure mitigation performance over the case when the TMD is passive with maximum available damping $de = 64.7$ N·s/m. Regarding the average value (I_A) of the protected structure response, the FBC strategy achieved a reduction of 14% compared to the passive system case. Also, the peak index was reduced by 3%. Although the protected structure with the undamped TMD must indicate an almost zero response between invariant points, in practice, it did not appear due to the continued presence of the mechanical friction between the TMD upper part and the solenoid. Compared to the system response

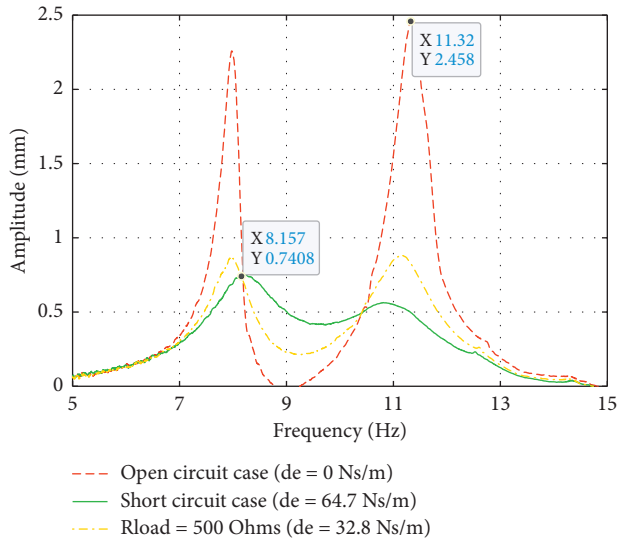

Figure 8: Protected structure with passive TMD amplitude-frequency response.

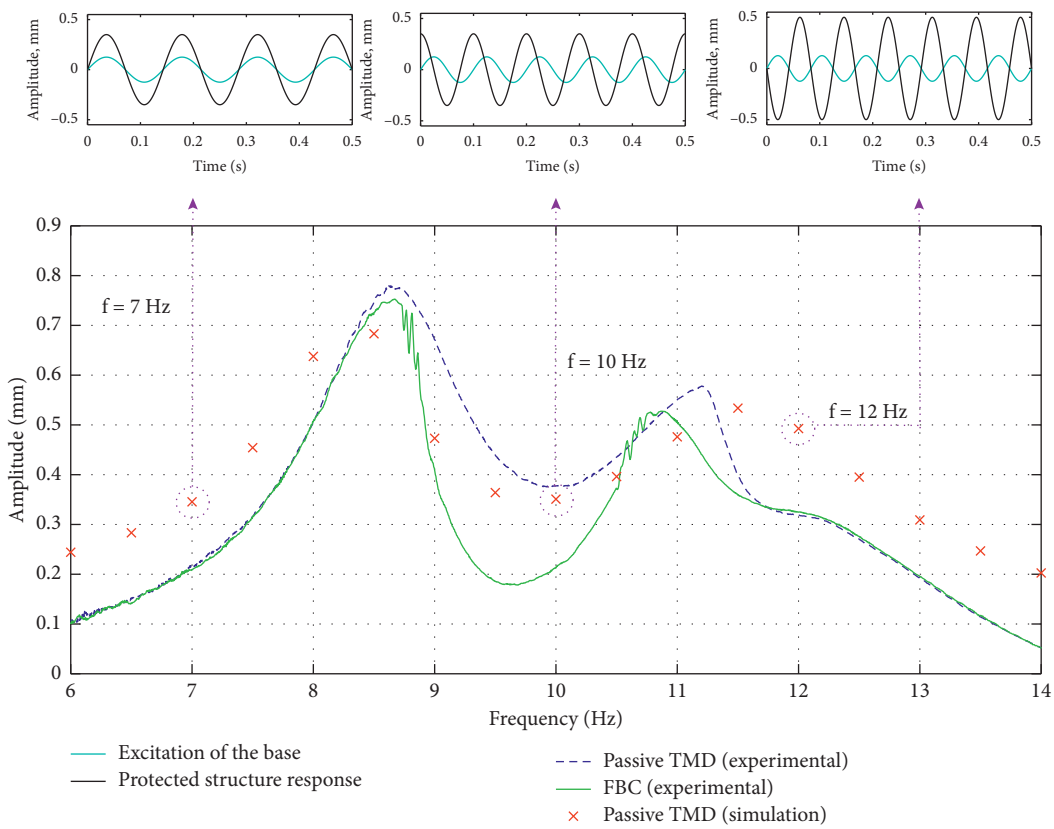

Figure 9: Frequency domain analysis of the protected structure.

given in Figure 4, the second peaks of the optimized case and the FBC strategy curves appeared lower as expected. This phenomenon can be explained by the presence of the second modal resonance frequency of the proposed TMD construction, which is mostly oscillating in a horizontal direction. It is worth noting that the control was executed with the compromised TMD amplitude. Based on the results shown in Figure 10, the TMD peak response for the FBC concept was increased by 14% compared to the passive TMD stroke length, with corresponding peak indices of $I_p = 3.03$ and 3.49, respectively. This fact should be considered for the correct estimation of the TMD stroke length for such a control policy.

Pinkaew and Fujino [12] found that the best semiactive approach resulted in a 20% reduction in the protected structure's displacement. Despite the marginally better efficiency (6% better than FBC), optimum control requires full state feedback measurement, which involves more sensors

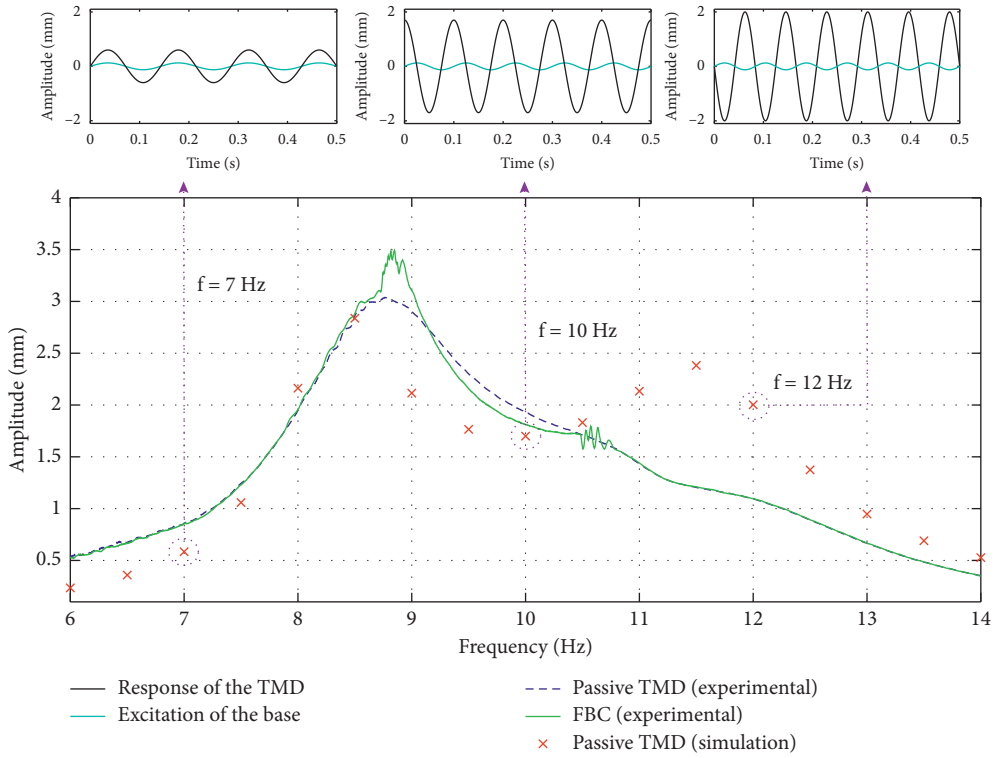

Figure 10: Frequency domain analysis of the TMD amplitude.

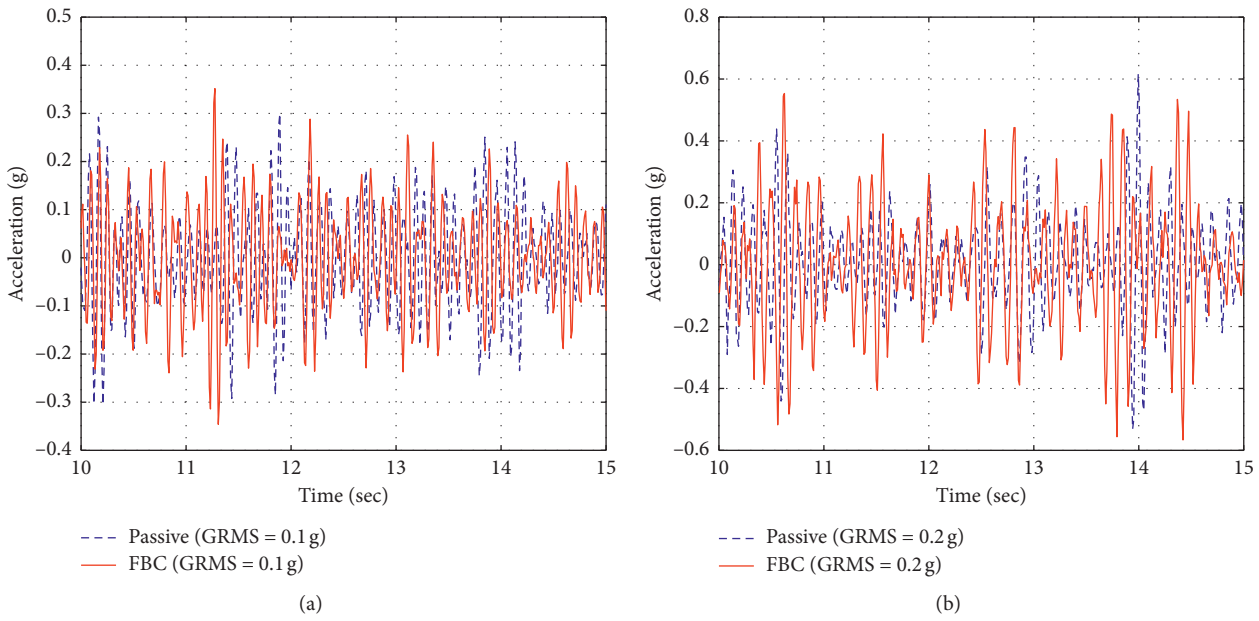

Figure 11: Acceleration response. (a) Protected structure. (b) TMD.

and increases the system complexity and cost significantly. Meanwhile, the suggested technique could be a cost-efficient and effective way to minimize unnecessary harmonic vibrations.

Finally, the controlled system performance was investigated under random vibration. Based on ISO 8608, the random vibration corresponding to the road irregularities class C was taken as an excitation [28]. The acceleration signal was exploited to estimate the performance of the system. However, the proposed algorithm failed to determine the excitation frequency properly. Consequently, the proposed FBC strategy did not have any advantage over the passive TMD system. The experimental results for the protected structure and TMD are given in Figure 11, where the gravitational acceleration $g = 9.81\ \text{m/s}^2$.

4. Conclusions

This paper proposed the FBC strategy for electromagnetic TMD applied to the protected structure exposed by harmonic excitation. The effectiveness of the proposed control strategy was validated experimentally under harmonic excitation of 5–15 Hz. The effects of the controlled TMD implementation were compared to the results of the passive TMD results. It was found that FBC policy has a significant effect on the mitigation of protected structures. The protected structure experienced a 14% reduction in average vibration, while the peak response was decreased by 3%. The findings demonstrated the benefit of using the suggested control technique only when there is harmonic excitation. This control policy can be used to prevent unwanted harmonic machine-induced vibrations in systems such as motors, driveshafts, flywheels, and rotors. The proposed control strategy did not show any differences under random vibration compared to the passive TMD. Therefore, as a future work for further research of the controlled TMD, it is recommended to investigate semiactive control strategies oriented on random excitations.

In future work, the proposed control algorithm for a Zener model system with substantial inductance should be developed further. Furthermore, the control scheme can be improved to be used by devices that are subject to stochastic vibration.

Data Availability

The data used to support the findings of this study are available from the corresponding author upon request.

Conflicts of Interest

The authors declared no potential conflicts of interest with respect to the research, authorship, and/or publication of this article.

References

[1] I. Takamoto, M. Abe, Y. Hara, T. Nakahara, K. Otsuka, and K. Makihara, "Predictive switching vibration control based on harmonic input formulation," *Sensors and Actuators A: Physical*, vol. 315, p. 112271, 2020.

[2] J. Wang, "Active restricted control for harmonic vibration suppression," *International Journal of Structural Stability and Dynamics*, vol. 19, no. 12, p. 1971007, 2019.

[3] Y. Zhang, K. Liu, and Z. Zhang, "Harmonic vibration suppression for magnetically suspended flywheel with rotor unbalance and sensor runout," *AIP Advances*, vol. 8, no. 10, p. 105207, 2018.

[4] J.-S. Bae, J.-H. Hwang, D.-G. Kwag, J. Park, and D. J. Inman, "Vibration suppression of a large beam structure using tuned mass damper and eddy current damping," *Shock and Vibration*, vol. 201410 pages, 2014.

[5] G. Nerubenko, *Vibration Energy Harvesting Damper in Vehicle Driveline*, SAE International, Warrendale, PA, USA, 2019.

[6] H. Gao, C. Wang, C. Huang, W. Shi, and L. Huo, "Development of a frequency-adjustable tuned mass damper (FATMD) for structural vibration control," *Shock and Vibration*, vol. 2020, Article ID 9605028, , 2020.

[7] F. Beltrán-Carbajal, "Variable frequency harmonic vibration suppression using active vibration absorption," *Revista Facultad de Ingenier'\ia Universidad de Antioquia*, vol. 73, pp. 144–156, 2014.

[8] M. Maślanka, "Measured performance of a semi-active tuned mass damper with acceleration feedback," in *Proceedings of the Active and Passive Smart Structures and Integrated Systems-Meeting 2017*, Portland, OR, USA, March 2017.

[9] I. Nishimura, T. Kobori, M. Sakamoto, N. Koshika, K. Sasaki, and S. Ohrui, "Active tuned mass damper," *Smart Materials and Structures*, vol. 1, no. 4, pp. 306–311, 1992.

[10] M.-H. Chey, J. G. Chase, J. B. Mander, and A. J. Carr, "Semiactive tuned mass damper building systems: design," *Earthquake Engineering \& Structural Dynamics*, vol. 39, no. 2, pp. 119–139, 2010.

[11] U. Aldemir, "Optimal control of structures with semiactive-tuned mass dampers," *Journal of Sound and Vibration*, vol. 266, no. 4, pp. 847–874, 2003.

[12] T. Pinkaew and Y. Fujino, "Effectiveness of semi-active tuned mass dampers under harmonic excitation," *Engineering Structures*, vol. 23, no. 7, pp. 850–856, 2001.

[13] P. Y. Lin, L. L. Chung, and C. H. Loh, "Semiactive control of building structures with semiactive tuned mass damper," *Computer-Aided Civil and Infrastructure Engineering*, vol. 20, no. 1, pp. 35–51, 2005.

[14] F. Ricciardelli, A. Occhiuzzi, and P. Clemente, "Semi-active tuned mass damper control strategy for wind-excited structures," *Journal of Wind Engineering and Industrial Aerodynamics*, vol. 88, no. 1, pp. 57–74, 2000.

[15] M. Rosół and P. Martynowicz, "Implementation of the LQG controller for a wind turbine tower-nacelle model with an mr tuned vibration absorber," *Journal of Theoretical and Applied Mechanics*, vol. 54, no. 4, pp. 1109–1123, 2016.

[16] J.-H. Koo, M. Ahmadian, M. Setareh, and T. Murray, "In search of suitable control methods for semi-active tuned vibration absorbers," *Journal of Vibration and Control*, vol. 10, no. 2, pp. 163–174, 2004.

[17] L. D. Viet, N. B. Nghi, N. N. Hieu, D. T. Hung, N. N. Linh, and L. X. Hung, "On a combination of ground-hook controllers for semi-active tuned mass dampers," *Journal of Mechanical Science and Technology*, vol. 28, no. 6, pp. 2059–2064, 2014.

[18] L.-L. Chung, Y.-A. Lai, C.-S. Walter Yang, K.-H. Lien, and L.-Y. Wu, "Semi-active tuned mass dampers with phase control," *Journal of Sound and Vibration*, vol. 332, no. 15, pp. 3610–3625, 2013.

[19] C. Moutinho, "Testing a simple control law to reduce broadband frequency harmonic vibrations using semi-active tuned mass dampers," *Smart Materials and Structures*, vol. 24, p. 055007, 2015.

[20] S. Kopylov, Z. Chen, and M. A. Abdelkareem, "Acceleration based ground-hook control of an electromagnetic regenerative tuned mass damper for automotive application," *Alexandria Engineering Journal*, vol. 59, no. 6, pp. 4933–4946, 2020.

[21] X. Tang and L. Zuo, "Simultaneous energy harvesting and vibration control of tall buildings using electricity-generating tuned mass dampers," *Journal of Intelligent Material Systems and Structures*, vol. 23, no. 18, 2012.

[22] S. Kopylov, Z. Chen, and M. A. Abdelkareem, "Back-iron design-based electromagnetic regenerative tuned mass damper," *Proceedings of the Institution of Mechanical Engineers, Part K: Journal of Multi-Body Dynamics*, vol. 234, no. 3, 2020.

[23] W. Minnemann Kuhnert, A. Cammarano, M. Silveira, and P. J. Paupitz Goncalves, "Optimum design of electromechanical vibration isolators," *Journal of Vibration and Control*, vol. 27, no. 1-2, 2021.

[24] D. Ning, H. Du, S. Sun, W. Li, and W. Li, "An energy saving variable damping seat suspension system with regeneration capability," *IEEE Transactions on Industrial Electronics*, vol. 65, no. 10, pp. 8080–8091, 2018.

[25] J. P. Den Hartog, *Mechanical Vibrations*, Courier Corporation, Chelmsford, MA, USA, 1985.

[26] W. M. Kuhnert, A. Cammarano, M. Silveira, and P. J. Gonçalves, "Synthesis of viscoelastic behavior through electromechanical coupling," *Journal of Vibration Engineering & Technologies*, vol. 9, pp. 367–379, 2021.

[27] M. J. Brennan, A. Carrella, T. P. Waters, and V. Lopes Jr, "On the dynamic behaviour of a mass supported by a parallel combination of a spring and an elastically connected damper," *Journal of Sound and Vibration*, vol. 309, no. 3-5, pp. 823–837, 2008.

[28] M. A. A. Abdelkareem, L. Xu, X. Guo et al., "Energy harvesting sensitivity analysis and assessment of the potential power and full car dynamics for different road modes," *Mechanical Systems and Signal Processing*, vol. 110, pp. 307–332, 2018.